Determination of stress, strain, and elemental distribution within In(Ga)As quantum dots embedded in GaAs using advanced transmission electron microscopy

Nikolay Cherkashin, Shay Reboh, Martin Hÿtch, Alain Claverie, V.V. Preobrazhenskii, M.A. Putyato, B.R. Semyagin, V.V. Chaldyshev

Determination of stress, strain, and elemental distribution within In(Ga)As quantum dots embedded in GaAs using advanced transmission electron microscopy

N. Cherkashin, S. Reboh, M. J. Hÿtch, A. Claverie, V. V. Preobrazhenskii, M. A. Putyato, B. R. Semyagin, and V. V. Chaldyshev

Citation: Appl. Phys. Lett. **102**, 173115 (2013); doi: 10.1063/1.4804380
View online: https://doi.org/10.1063/1.4804380
View Table of Contents: http://aip.scitation.org/toc/apl/102/17
Published by the American Institute of Physics

Determination of stress, strain, and elemental distribution within In(Ga)As quantum dots embedded in GaAs using advanced transmission electron microscopy

N. Cherkashin,[1,a)] S. Reboh,[1,2] M. J. Hÿtch,[1] A. Claverie,[1] V. V. Preobrazhenskii,[3] M. A. Putyato,[3] B. R. Semyagin,[3] and V. V. Chaldyshev[4]
[1]*CEMES, CNRS UPR 8011 and Université de Toulouse, 29 rue Jeanne Marvig, 31055 Toulouse, France*
[2]*CEA-Leti, 17 rue des Martyrs, 38054 Grenoble, France*
[3]*Rzhanov Institute of Semiconductor Physics, Siberian Branch of the RAS, 13 Ac. Lavrentieva, 630090 Novosibirsk, Russia*
[4]*Ioffe Physico-Technical Institute of the RAS, 26 Politekhnicheskaya Str., 194021 St. Petersburg, Russia*

(Received 23 March 2013; accepted 24 April 2013; published online 3 May 2013)

Non-truncated pyramidal In(Ga)As quantum dots (QDs) embedded in GaAs were obtained by a combination of low temperature/high rate GaAs covering of InAs QDs. We use advanced transmission electron microscopy to study the composition and mechanics of the objects. Results from the core region of a sliced QD, and from an entire object, are consistent and complementary allowing the development of accurate models describing the 3D shape, chemical distribution, elastic strains and stresses in the QD, wetting layer, and matrix. The measured structure develops an extremely compressive apex, reaching a vertical stress of −8 GPa and horizontal stress of −6.2 GPa. © *2013 AIP Publishing LLC*. [http://dx.doi.org/10.1063/1.4804380]

Quantum dots (QDs) are nano-objects exhibiting 3D quantum confinement of charge carriers. The atomic-like properties emerging from these systems have been exploited, for example, for advanced electronics and optoelectronics.[1–4] Structural aspects, such as the morphology,[5,6] the spatial distribution of chemical elements,[7,8] and the elastic strain,[9–11] influence the electronic confinement properties of the system.[12] When QDs are embedded in a matrix, mechanical strain can also be used to create spatial ordering using elegant bottom-up approaches.[13–15] Therefore, understanding the physics that correlate strain, morphology, and composition of QDs is extremely complex, but essential for technology.[16,17] A necessary but challenging step towards this goal is to provide accurate quantitative descriptions of the structure of such small objects.

Here, we combine two techniques of advanced transmission electron microscopy (TEM) to study coherent In(Ga)As QDs in a GaAs matrix. Extremely thin (<15 nm) specimens, where the QDs were sectioned, were prepared to be studied by geometric phase analysis (GPA)[18] of high-resolution TEM (HRTEM) images. With this, we assess the core region of the object. Dark-field electron holography (DFEH)[19] was used to study complete QDs embedded in a thick TEM foil. In both cases, to determine the geometry of the studied QD and to decouple the chemical strains from elastic strains, we used finite element methods (FEM) to model the structures. The accurate characterization of the system obtained here allows us to provide a precise 3D description of the QD and surrounding matrix including a compositional map, elastic strain/stress fields, and elastic energy.

The material was fabricated by molecular beam epitaxy (MBE). Five monolayers (MLs) of InAs were deposited at a rate of 0.05 ML/s on semi-insulating (001) GaAs substrates kept at 460 °C. This creates a highly strained layer of InAs. An elastic relaxation process leads to the formation of 3D island-like pyramidal QDs of square base with edges running parallel to ⟨010⟩ directions of the crystal matrix.[20] The exposed facets of the objects are generally of {101} type.[21] Without changing the processing temperature, the QDs were buried by overgrowing 30 nm of GaAs at a deposition rate of 0.3 nm/s.

Cross-sectional $(1\bar{1}0)$ TEM specimens were prepared by tripod mechanical polishing followed by Ar^+ ion milling. The experiments were performed at 200 kV in the SACTEM-Toulouse (Tecnai-FEI) microscope, equipped with image aberration corrector and rotatable electrostatic biprism. In a complementary way: (i) high-resolution TEM micrographs were taken in a thin region of the TEM lamella (10 ± 3 nm), where the QDs were partially cut, and strain maps were obtained with a spatial resolution of 1 nm, and (ii) dark-field electron holograms were obtained in a sufficiently thick region (40 ± 3 nm) where we found QDs completely embedded in the foil. In the latter case, the strain maps were obtained with a spatial resolution of 2.5 nm. Holograms were recorded after exciting the diffraction vectors $g = 111$ and $g = \bar{1}\bar{1}1$. The high-resolution TEM images and dark-field electron holograms were analyzed using GPA Phase 3.5 and HoloDark 1.0 (HREM Research, Inc.), plug-ins for the image processing package Digital Micrograph (Gatan Inc.). The measured strain field maps ε_{ij}^{rel} (with i, j = x, z being coordinates in the image plane, perpendicular to the observation axis y) are hereafter presented with reference to the unstrained GaAs lattice, indicated by the superscript "*rel*." With respect to the GaAs substrate, we define the coordinate system as $x//[110]$, $y//[1\bar{1}0]$, and $z//[001]$, where the z-axis corresponds to the direction normal to the surface of the substrate.

The interpretation of the results in terms of elastic strain and chemical composition requires a combination of

[a)]Author to whom correspondence should be addressed. Electronic mail: nikolay.cherkashin@cemes.fr

experiments and modeling. Here, we developed analytical and finite element method based calculations considering the full anisotropy of the system and materials. When modeling results obtained by TEM, the thickness of the specimen is a critical factor which induces elastic relaxation of the system.[22,23] The foil thicknesses were deduced from extinction fringe contrast excited in the dark-field TEM mode. The input variables in the models include therefore: (i) the thickness of the TEM foil; (ii) the 3D morphology of the QD; (iii) the spatial distribution of Ga and In in the In(Ga)As QD and in the wetting layer (WL); and (iv) the position of the QD along the thickness of the TEM lamella.

The results from the model were compared to the measured strains according to a strict protocol. First, the maps of displacement field u_x and u_z generated by the code were averaged over the thickness of the lamella and projected along the viewing direction. The projected images were used to generate a virtual high-resolution TEM pictograph formed by two sets of lattice fringes. The results were then analyzed exactly as the recorded experimental data, i.e., by defining the same region as a reference for strain, and the same spatial resolution for the analysis. Once the agreement between the measured and calculated strain is satisfactory, by simply modifying the lateral dimensions and the boundary conditions of the model, we can describe the original bulk structure.

Figure 1(a) shows, in a region between two QDs, the map of ε_{zz}^{rel} of the wetting layer obtained by geometric phase analysis of a high-resolution TEM image. The positive values indicate that, along the z direction, the wetting layer has a larger interplanar distance than the matrix. The horizontal component ε_{xx}^{rel} is null (not shown), the layer is hence pseudomorphic to the GaAs lattice along the x direction, i.e., compressively strained in relation to its proper relaxed lattice. The solid line in Fig. 1(b) corresponds to a vertical profile extracted from Fig. 1(a). The peak value of strain reaches about 2%. The shape of the curve is asymmetric, having an abrupt variation opposed to a more gradual behavior. The wetting layer is thus not composed of pure InAs, otherwise an abrupt change of strain at the interfaces of wetting layer/matrix would be observed.

For 2D layers much thinner than the foil thickness, as here, the effect of the thin foil relaxation is negligible.[24] Therefore, to model the strain in the wetting layer is sufficient to assume a plane stress configuration where σ_{zz} perpendicular to the free surface vanishes. Combining elasticity and Vegard's law, the $\varepsilon_{zz}^{rel}(z)$ as function of In concentration $f_{WL}^{\mathrm{In}}(z)$ reads then as

$$\varepsilon_{zz}^{rel}(z) = \frac{a^{\mathrm{InAs}} - a^{\mathrm{GaAs}}}{a^{\mathrm{GaAs}}} \left(2\frac{C_{12}^{\mathrm{InGaAs}}(z)}{C_{11}^{\mathrm{InGaAs}}(z)} + 1\right) f_{WL}^{\mathrm{In}}(z) \approx 0.14 f_{WL}^{\mathrm{In}}(z), \quad (1)$$

where $C_{12}^{\mathrm{InGaAs}}(z)$ and $C_{11}^{\mathrm{InGaAs}}(z)$ are the elastic constants of the $In_xGa_{1-x}As$ alloy, a^{InAs} and a^{GaAs} are the lattice parameters of unstrained InAs and GaAs. The strain profile presented in dashed line in Fig. 1(b) was obtained by describing $f_{WL}^{\mathrm{In}}(z)$ as a probability density function of lognormal distribution given by

$$f_{WL}^{\mathrm{In}}(z) = A\frac{1}{zB\sqrt{2\pi}} e^{-\frac{(\ln z-\mu)^2}{2B^2}}, \quad (2)$$

where the best fit to the experiments was found for $A = 0.69 \pm 0.01$, $\mu = 1.25 \pm 0.05$, and $B = 0.70 \pm 0.02$. The maximum value of $f_{WL}^{\mathrm{In}}(z)$ is $14.3 \pm 0.5\%$, and the integration of the function gives the total amount of In in the wetting layer. In units of (002) interplanar distance, it corresponds here to 2.3 ± 0.3 MLs of InAs. It means that, from the originally deposited 5 MLs of InAs, around 2.7 MLs contributed to the formation of QDs and/or out-diffused from the system.

Figures 2(a) and 2(b) are maps of ε_{zz}^{rel} and ε_{xx}^{rel} of a QD, obtained from geometric phase analysis of a high-resolution TEM micrograph. Positive ε_{zz}^{rel} values are delimited in a triangular region corresponding to the 2D projection of a pyramidal structure. Tensile peak values appear in the upper area of the object, and negative ones are identified above the apex and below the base of the triangle. The ε_{xx}^{rel} component is predominantly positive. It emerges from an epicenter situated in a region corresponding to the upper area of the triangle in Fig. 2(b). Figures 2(c) and 2(d) provide a visualization of our calculated strain maps. Profiles extracted from the

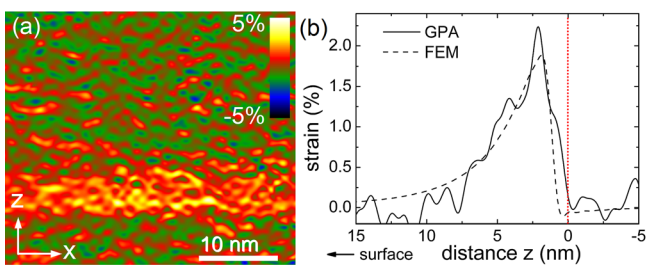

FIG. 1. (a) Map of ε_{zz}^{rel} obtained by geometric phase analysis of a high-resolution TEM micrograph of the wetting layer in a region between two QDs. A vertical profile of the strain map in (a) is displayed in (b) (solid line) together with the calculated one using Eqs. (1) and (2) (dashed line). The values are averaged over a stripe of 30 nm parallel to the surface. Zero in the distance axis corresponds to the original wetting layer/matrix interface.

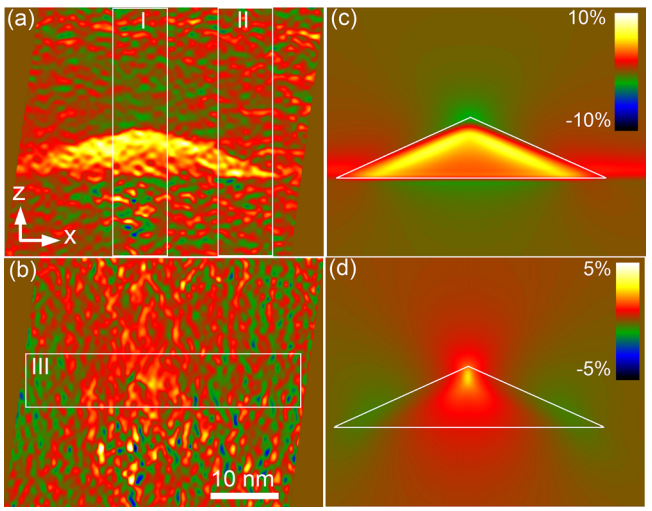

FIG. 2. Maps of (a) ε_{zz}^{rel} and (b) ε_{xx}^{rel} obtained by geometric phase analysis of a high-resolution TEM micrograph of a QD. The regions I, II, and III delimited by the full lines were used to extract the profiles in Fig. 3. The calculated strain maps are in (c) for ε_{zz}^{rel} and (d) for ε_{xx}^{rel}. The triangles depicted by full white lines in (c) and (d) indicate the boundaries of the QD considering a vertical cut passing through its apex.

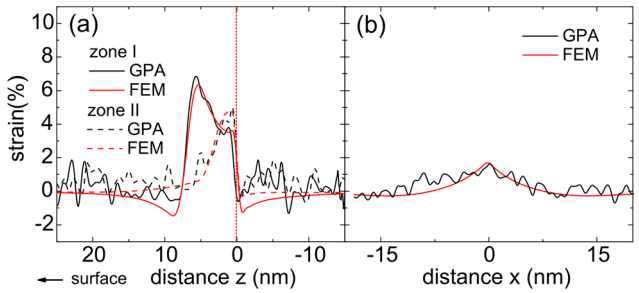

FIG. 3. Profiles of (a) ε_{zz}^{rel} and (b) ε_{xx}^{rel} extracted from the experimental and calculated images in Fig. 2. Black lines refer to experimental profiles and red lines for the calculated ones. The zero stands for the QD/matrix interface in (a) and for the central axis of the QD in (b).

regions I and II, delimited by the full lines in Fig. 2(a), are plotted in Fig. 3(a) along with the corresponding calculated ones. The values of ε_{zz}^{rel} in region I decrease from the upper region of the QD to its base. In region II, the maximum of strain is close to the QD/substrate interface. Fig. 3(b) shows the profiles extracted from the selected area in Fig. 2(b). The values of ε_{xx}^{rel} are smaller than ε_{zz}^{rel}, as consequence, the signal/noise ratio is lower.

The calculated profiles show the quantitative agreement between the model we propose and the experimental data. In the calculations, the QD is centered in a 10 nm thick foil, and embodied by a four-fold pyramidal volume of 9 nm height and a square base with side lengths of 28 nm parallel to in-plane $\langle 010 \rangle$ directions. In contrast with the original structure, having $\{101\}$ facets with $\langle 111 \rangle$ edges before GaAs overgrowth,[20,21] the buried QDs are characterized by $\{203\}$ facets with $\langle 332 \rangle$ edges.

The In distribution $C_{QD}^{\mathrm{In}}(x,y,z)$ in the QD is here described by

$$C_{QD}^{\mathrm{In}}(x,y,z) = c_{base}^{\mathrm{In}} + \left(f_{facet}^{\mathrm{In}}(z) - c_{base}^{\mathrm{In}}\right) \frac{z}{\frac{L}{\sqrt{2}} - x - y} \frac{L}{\sqrt{2}H}, \tag{3}$$

where the origin coordinate (0,0,0) situates at the center of the QD base and $f_{facet}^{\mathrm{In}}(z) = c_{facet}^{\mathrm{In}} + (1 - c_{facet}^{\mathrm{In}})\sqrt{\frac{z}{H}}$ gives the In distribution along the facets. The constants $c_{facet}^{\mathrm{In}} = 0.25$ and $c_{base}^{\mathrm{In}} = 0.4$ stand for the In concentration in the facets and the base of the object for z = 0. Comparing experiment with a series of finite element method calculations (not shown) where we varied the composition, shape, and dimensions of the QD, we estimate our precision to be ±5% for the In composition, ±0.5 nm and ±2 nm, respectively, for the height and lateral dimensions of the QD.

In the second part of our experiments, we used dark-field electron holography to study a complete QD embedded in the TEM foil. The technique allows imaging larger fields of view and, consequently, provides an enhanced perception of the general picture. The results are exposed in Figs. 4(a)–4(c). They show roughly similar strain distributions to the ones found by high-resolution TEM (Fig. 2); however, for example, in Fig. 4(a), the slightly compressive ε_{xx}^{rel} regions in the right and left sides of the tensile epicenter are well portrayed. It is the same case for the compressive areas above and below the QD in Fig. 4(b), and for the continuity

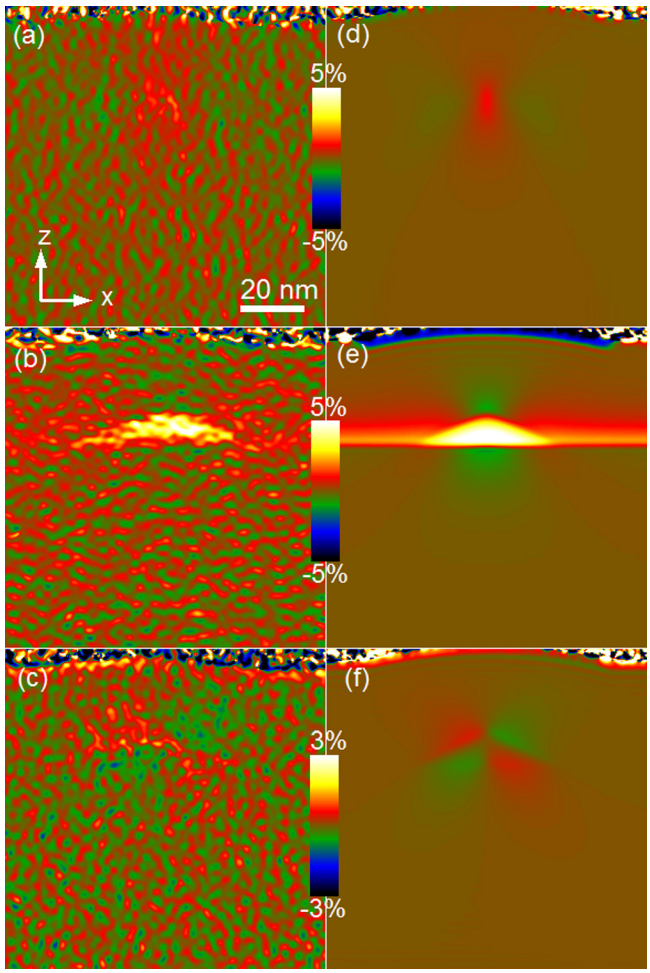

FIG. 4. (a) ε_{xx}^{rel}, (b) ε_{zz}^{rel}, and (c) ε_{zx}^{rel} components of the QD strain field mapped by dark-field electron holography. The corresponding calculated maps are shown in (d) for ε_{xx}^{rel}, (e) for ε_{zz}^{rel}, and (f) for ε_{xz}^{rel}.

between QD and wetting layer. We also highlight that the distribution of shear strain ε_{xz}^{rel}, which presents relatively lower intensities, is well discerned in Fig. 4(c). The image presents an inverse mirror symmetry with respect to the central vertical axis of the QD.

The finite element method model developed to describe the high-resolution TEM results is applied here to verify its consistency. The only modification was the QD dimensions, to account for the larger base length of 34 nm and height of 11 nm of the observed object. The calculated strains are confronted to the experiments in Figs. 4(d)–4(f) showing the agreement of the model we propose with the fabricated structures. We can now consider that our model describes correctly the strains and the distribution of chemical elements in the system. Therefore, we explore the calculations to provide not only the 3D shape and the distribution of composition in the QDs but as well the real stresses and decouple elastic and chemical strains. Elastic strains are defined with respect to the relaxed state of material with the specific composition at any given point of the volume.

To present the results for the bulk structure, we extended the matrix surrounding the QD to a distance equivalent to twice its base-diagonal. Symmetry conditions allowed us to calculate results from one quarter of the structure. The lower boundary plane in the substrate was set to have zero vertical

displacement. The In relative composition (Eq. (3)) is plotted in Fig. 5(a) where z is the vertical symmetry axis of the QD. The concentration of In increases from the base of the QD to its apex, and from the center to the facets in the upper part of the QD. The average In concentration ⟨C⟩ obtained by the integration of Eq. (3) over the QD volume is given as

$$\langle C\rangle = \left(\frac{HL^2}{3}\right)^{-1} 4\int_H^0 \int_{\frac{L}{\sqrt{2}}\left(1-\frac{z}{H}\right)}^{0} \int_0^{\frac{L}{\sqrt{2}}\left(1-\frac{z}{H}\right)-y} C_{QD}^{\mathrm{In}}(x,y,z)dxdydz. \tag{4}$$

For the studied QDs where L/H ≈ 3.1, $c_{facet}^{\mathrm{In}} = 0.25$ and $c_{base}^{\mathrm{In}} = 0.4$, the $\langle C\rangle = 0.53$. The average composition of the dots is $In_{0.53}Ga_{0.47}As$.

Figure 5(b) gives the general picture of the in-plane dilatation defined as $\frac{1}{2}(\varepsilon_{xx}+\varepsilon_{yy})$. The distributions of out-of-plane stress σ_{zz} and in-plane stress, given by $\frac{1}{2}(\sigma_{xx}+\sigma_{yy})$, are shown in Figs. 5(c) and 5(d). The contour plots in the stress maps represent the regions of iso-value, giving a clue on the spatial distribution of stresses. In contrast to the tensile strains obtained by geometric phase analysis of high-resolution TEM images and by dark-field electron holography, Fig. 5 shows that the true elastic strains and stresses in the QD are predominantly compressive. At the apex composed of pure InAs, values rise to a maximum in-plane compression of −4% or −6.2 GPa. In a counter intuitive manner, even if the system is free to relax over the free surface of the wafer, i.e., towards the z-direction, the local configuration of the structure makes σ_{zz} considerably higher than the in-plane stress at the apex, achieving up to −8 GPa. Elsewhere, the QD is also characterized by a hydrostatic compression of the lattice, however, with the in-plane stress higher than σ_{zz}.

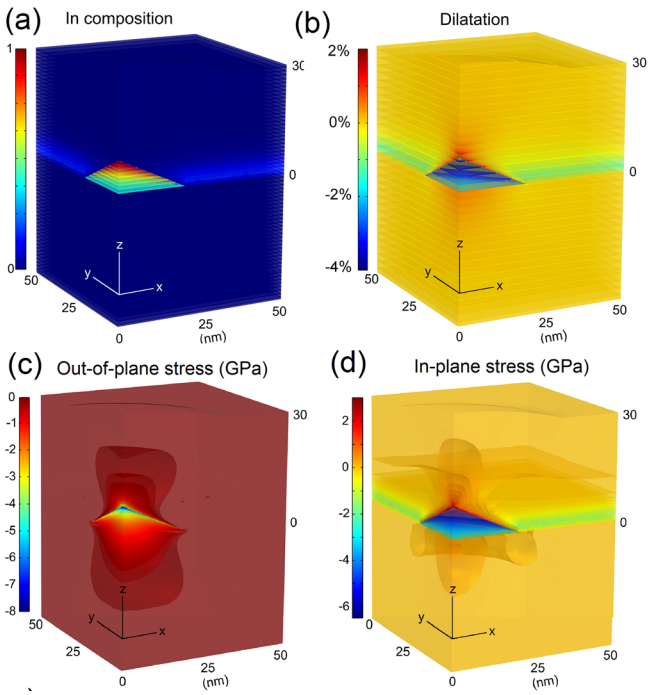

FIG. 5. 3D finite element method calculations presented for a quarter of the structure showing (a) the In distribution; (b) the in-plane dilatation of the lattice; (c) the out-of-plane stress σ_{zz}; and (d) the in-plane component of stress.

Finally, we have calculated the average density of elastic energy E of the structure, and compared it with an island with a homogeneous $In_{0.53}Ga_{0.47}$ As distribution of chemical elements over the QD volume. Calculations show that E within the QD is 7.75% lower for the homogeneous case. If we take into account the surrounding GaAs (defined in Fig. 5) the trend is similar, with a reduction of 4.4% with respect to the experimental configuration. To explain this phenomenon, we must consider the particularity of the QD formation and overgrowth processes.

After InAs deposition, the strained 2D layer develops into 3D pyramids by the Stranski-Krastanow mechanism, allowing the material to restore its bulk lattice parameter at the apex and the edges of the object. During the initial stage of the GaAs deposition, GaAs preferentially covers the wetting layer between QDs. The intermixing of Ga and In in the base of the structure has the effect of modifying the QD shape and allows the reduction of the mismatch at the QD/substrate interface.[16,25,26] The relatively low GaAs growth temperature used here avoids a dissolution of the pyramid apex enriched by In.[25,26] As a consequence, once completely covered, the largest difference of lattice parameters between the QD and surrounding material is introduced at the apex of the structure. Due to the disproportionate difference of matrix/apex volumes, extremely high compressive stresses are generated in this limited spatial region of the QD. This phenomenon causes a substantial increase of the strain energy of the system. The final structure therefore results from an intricate interplay between thermodynamics and kinetics effects intimately related to the QD formation and overgrowth regimes.

In conclusion, we used high-resolution TEM and dark-field electron holography to study the composition and mechanics of In(Ga)As QDs embedded in GaAs. The results obtained from a core region of the QD and from a complete object are consistent and complementary. We observed InGaAs alloying in the central region of the QD while its apex and outer facets contain a high In concentration. This situation, which would be favorable from a thermodynamic point of view for an uncovered QD, develops extremely high compressive stresses when covered by GaAs. We attribute the creation of this structure to the QD formation and GaAs overgrowth at the relatively low temperature. We developed a precise and accurate finite element method model describing the 3D distribution of elastic strains and stresses in the QD, wetting layer and their vicinity. The given analytical description of the In distribution for the QD and wetting layer provides as well a flexible adjustment of a finite element method model for QDs grown at other regimes than studied here.

The research was supported by the CNRS and the Russian Foundation for Basic Research via PICS 5577 program and by the French National Agency (ANR) in the frame of its program in Nanosciences and Nanotechnologies (HD STRAIN Project No. ANR-08-NANO-0 32). The authors thank N. A. Bert, A. E. Romanov, and A. L. Kolesnikova for useful discussions. S. Reboh is grateful to the support of the Brazilian agency CAPES under Project No. 2358-09-3.

[1]N. N. Ledentsov, M. Grundmann, F. Heinrichsdorff, D. Bimberg, V. M. Ustinov, A. E. Zhukov, M. V. Maximov, Zh. I. Alferov, and J. A. Lott, IEEE J. Sel. Top. Quantum Electron. **6**(3), 439–451 (2000).
[2]J. He, H. J. Krenner, C. Pryor, J. P. Zhang, Y. Wu, D. G. Allen, C. M. Morris, M. S. Sherwin, and P. M. Petroff, Nano Lett. **7**, 802–806 (2007).
[3]C.-C. Chang, Y. D. Sharma, Y.-S. Kim, J.-A. Bur, R. V. Shenoi, S. Krishna, D. Huang, and S.-Y. Lin, Nano Lett. **10**, 1704–1709 (2010).
[4]C. M. Morris, D. Stehr, H. Kim, T. Truong, C. Pryor, P. M. Petroff, and M. S. Sherwin, Nano Lett. **12**, 1115–1120 (2012).
[5]N. N. Ledentsov, V. A. Shchukin, D. Bimberg, V. M. Ustinov, N. A. Cherkashin, Y. G. Musikhin, B. V. Volovik, G. E. Cirlin, and Z. I. Alferov, Semicond. Sci. Technol. **16**(6), 502–506 (2001).
[6]N. A. Cherkashin, M. V. Maksimov, A. G. Makarov, V. A. Shchukin, V. M. Ustinov, N. V. Lukovskaya, Y. G. Musikhin, G. E. Cirlin, N. A. Bert, Z. I. Alferov, N. N. Ledentsov, and D. Bimberg, Semiconductors **37**(7), 861–865 (2003).
[7]D. Litvinov, D. Gerthsen, A. Rosenauer, M. Schowalter, T. Passow, P. Feinäugle, and M. Hetterich, Phys. Rev. B **74**(16), 165306 (2006).
[8]D. Litvinov, H. Blank, R. Schneider, D. Gerthsen, T. Vallaitis, J. Leuthold, T. Passow, A. Grau, H. Kalt, C. Klingshirn, and M. Hetterich, J. Appl. Phys. **103**(8), 083532 (2008).
[9]J. H. Devies, J. Appl. Phys. **84**(3), 1358–1365 (1998).
[10]V. A. Shchukin, N. N. Ledentsov, and D. Bimberg, *Epitaxy of Nanostructures* (Springer, Berlin, 2002).
[11]D. Cooper, J.-L. Rouviere, A. Béché, S. Kadkhodazadeh, E. S. Semenova, K. Yvind, and R. Dunin-Borkowski, Appl. Phys. Lett. **99**, 261911 (2011).
[12]M. Holm, M.-E. Pistol, and C. Pryor, J. Appl. Phys. **92**(2), 932–936 (2002).
[13]G. S. Solomon, J. A. Trezza, A. F. Marshall, and J. S. Harris, Jr., Phys. Rev. Lett. **76**, 952 (1996).
[14]V. N. Nevedomskii, V. V. Chaldyshev, N. A. Bert, V. V. Preobrazhenskii, M. A. Putyato, and B. R. Semyagin, Semiconductors **43**(12), 1617–1621 (2009).
[15]O. G. Schmidt, C. Deneke, S. Kiravittaya, R. Songmuang, H. Heidemeyer, Y. Nakamura, R. Zapf-Gottwick, C. Muller, and N. Y. Jin-Phillipp, IEEE J. Sel. Top. Quantum Electron. **8**(5), 1025–1034 (2002).
[16]Y. Tu and J. Tersoff, Phys. Rev. Lett. **98**, 096103 (2007).
[17]C. Deneke, A. Malachias, A. Rastelli, L. Merces, M. Huang, F. Cavallo, O. G. Schmidt, and M. G. Lagally, ACS Nano **6**(11), 10287–10295 (2012).
[18]M. J. Hÿtch, E. Snoeck, and R. Kilaas, Ultramicroscopy **74**, 131–146 (1998).
[19]M. J. Hÿtch, F. Houdellier, F. Hüe, and E. Snoeck, Nature **453**, 1086–1089 (2008).
[20]N. A. Bert, A. L. Kolesnikova, V. N. Nevedomsky, V. V. Preobrazhenskii, M. A. Putyato, A. E. Romanov, V. M. Seleznev, B. R. Semyagin, and V. V. Chaldyshev, Semiconductors **43**(10), 1387–1393 (2009).
[21]P. Kratzer, Q. K. K. Liu, P. Acosta-Diaz, C. Manzano, G. Costantini, R. Songmuang, A. Rastelli, O. G. Schmidt, and K. Kern, Phys. Rev. B **73**, 205347 (2006).
[22]M. Hytch, N. Cherkashin, S. Reboh, F. Houdellier, and A. Claverie, Phys. Status Solidi A **208**(3), 580–583 (2011).
[23]A. Claverie, N. Cherkashin, F. Hue, S. Reboh, F. Houdellier, E. Snoeck, and M. Hytch, ECS Trans. **33**(6), 47–58 (2010).
[24]N. Cherkashin, M. J. Hÿtch, E. Snoeck, F. Huë, J. M. Hartmann, Y. Bogumilowicz, and A. Claverie, Nucl. Instrum. Methods Phys. Res. B **253**, 145–148 (2006).
[25]N. Liu, J. Tersoff, O. Baklenov, A. L. Holmes, Jr., and C. K. Shih, Phys. Rev. Lett. **84**(2), 334 (2000).
[26]H. Eisele, A. Lenz, R. Heitz, R. Timm, M. Daühne, Y. Temko, T. Suzuki, and K. Jacobi, J. Appl. Phys. **104**, 124301 (2008).